

NUMERICAL SIMULATION OF RESISTANCE SPOT WELDING PROCESS USING FEA TECHNIQUE

C. Srikunwong^{*,**}, T. Dupuy^{*}, and Y. Bienvenu^{**}

ABSTRACT

2-D axisymmetric finite element models incorporating electrical-thermal and thermal-mechanical coupling procedures were developed for resistance spot welding (RSW) process simulation. A commercial finite element code, namely SYSWELD[®], was utilized for these simulation purposes. The coupling procedures can provide a more realistic and efficient computational approach accounting for the variation of contact size; particularly for the application of curved-face electrodes producing a spot weld. The temperature dependency characteristics and properties of both sheets and electrodes were also taken into account throughout the study. The welding schedules based on practical aspects of similar two- as well as three-sheet assemblies were considered for the entire of process. Not only the utilization of pulsed direct current but also that of pulsed alternating current was utilized in order to efficiently achieve the industrial protocol. The experimental study was centered on nugget formation. The validation for the nugget development was determined in the case of pulsed direct current welding.

The impact of pulsed alternating current welding combining supplementary post-heating pulses on the nugget size as well as on the thermal history was investigated. It was concluded that both heating and cooling rates depend strongly on the position of weld. The results of electrical-thermal analysis were discussed in view of the thermal history during welding, with particular regard for different types of welding current used.

INTRODUCTION

Resistance spot welding (RSW) is widely utilized as a joining technique for automobile structure due to flexibility, robustness and high-speed of process combining with very high quality joints at very low cost. Not only heavy gauge two-sheet assemblies are joined by this technique but also stack-up sheet assemblies can often be encountered in the application. In some cases of heavy gauge two-sheet joining, the use of a common continuous current signal is sometimes not efficient to construct the desired weldability lobe. The pulsed welding approach then becomes an other choice to achieve this purpose. The pulsed welding current based schedule is sometimes recommended for heavy gauge and stack-up assembly cases associated with some welding signal modification in order to improve weldability and mechanical properties of spot weld. The pulse current used can be medium frequency direct or alternating current pulse. Other adapted current signal such as down sloping, quenching or post-heating can be also introduced to a required welding current signal. These modifications become a common convenient technique for the improvement of weld mechanical-metallurgical properties in high strength steel joining (Ref. 1). The use of pulsed welding has many advantages in heavy gauge sheet joining including the stability of nugget development characteristics and the reduction of electrode wear.

* CRDM, Sollac Atlantique, ARCELOR Group, BP 2508, 59381, Dunkirk, France

** Ecole des Mines de Paris, BP 87, Evry Cedex, 91003, France

The recent development in finite element analysis for RSW numerical simulation is well documented in the literature (Refs. 2 and 3) showing that there is a significant change in the contact radii between electrode-to-sheet and sheet-to-sheet interfaces during welding stage. This has significant impacts on thermal history, nugget formation and thermal stresses in the assembly. Therefore, it is vital to implement a coupling procedure between electrical-thermal and thermal-mechanical modules in order to capture this physical interaction and produce a more realistic predictive model.

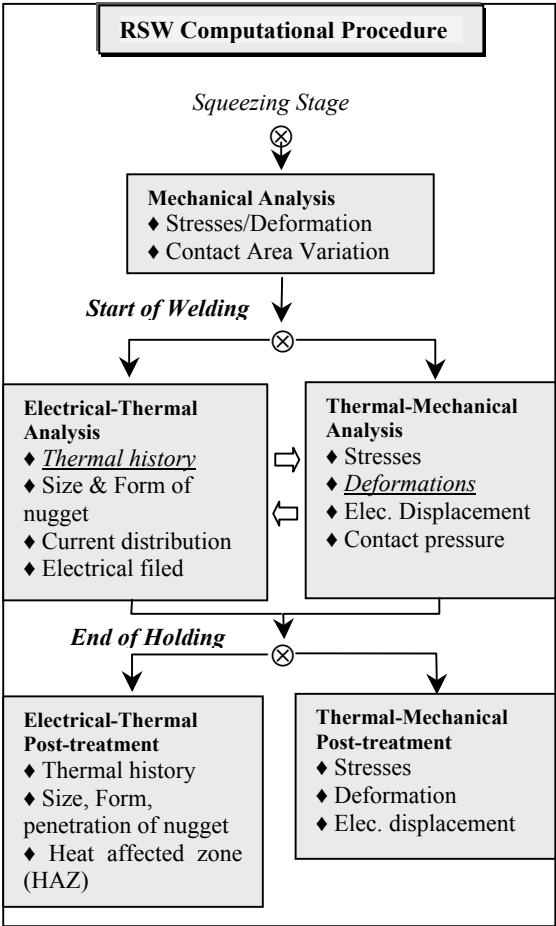


Figure 1: Schematic illustration of computational procedure

The aim of this study is to obtain a better understanding of the influence of process parameters for heavy gauge sheet joining with the use of pulsed welding current. The features of the coupling procedures can be described by loop sequential computational procedures of the nodal temperatures transferred from the electrical-thermal analysis to the thermo-mechanical analysis in order to compute the thermal stresses and assembly distortions. On the other hand, the stress distributions associated with assembly deformation are then transferred back to the next electro-thermal computation step in order to up-date the variation of the contact size and pressure. These successive sequential loops are cumulated until the end of RSW process. The computational procedure employed in this study is illustrated in fig. 1.

FORMULATION FOR MODELING

Structure Modeling

A representative assembly of electrode and sheet utilized for analysis as shown in fig. 2 illustrates a half axisymmetric finite element model for electrode and sheet assembly, which is considered for both electrical-thermal and thermal-mechanical analyses. 2-D axisymmetric models of two- and three-sheet joining incorporated with the curved face electrode of 6mm and 8mm.-diameter are constructed. Both electrical-thermal and mechanical contact elements are specially treated at electrode-to-sheet and sheet-to-sheet interfaces.

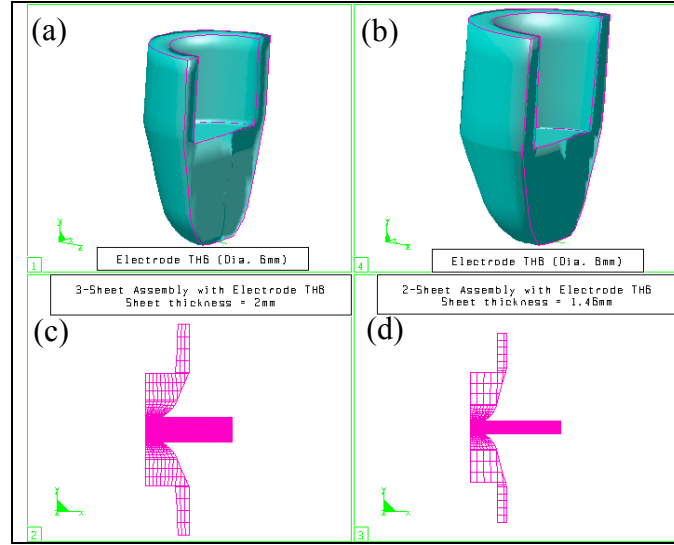


Figure 2: Illustration of structure mesh models used in analysis

Figure 2a: Curved-face electrode of 6mm-dia; Figure 2b: Curved-face electrode of 8mm-dia
Figure 2c: Three-sheet assembly mesh model; Figure 2d: Two-sheet assembly mesh model

Electrical-Thermal Modeling

RSW process is a resistance welding process governed by Joule heating effect with a concentration of the heat generation at the interface between two solid bodies in contact while passing the current. This heat further propagates into these bodies by conduction heat transfer mode associated with the imposed thermal boundary conditions. Electrical-thermal governing system equations are presented in (1) and (2):

$$\rho \frac{\partial H}{\partial t} - \text{div}(\lambda \cdot \text{grad}T) - \text{grad}V \cdot \sigma \cdot \text{grad}V - Q = 0 \quad (1)$$

$$\text{div}(\sigma \cdot \text{grad}V) = 0 \quad (2)$$

Where T, V are the temperature and the scalar electrical potential, respectively. ρ, λ and σ represent the density, the thermal conductivity and the electrical conductivity of the medium. The temperature dependency characteristics can be taken into account in these equations. H is the enthalpy also with a temperature dependency. The full coupling between electrical and thermal phenomena can be governed by the term $\text{grad}V \cdot \sigma \cdot \text{grad}V$ in the heat equation. The modeled alternating current signal used in the analysis is shown in fig. 3a.

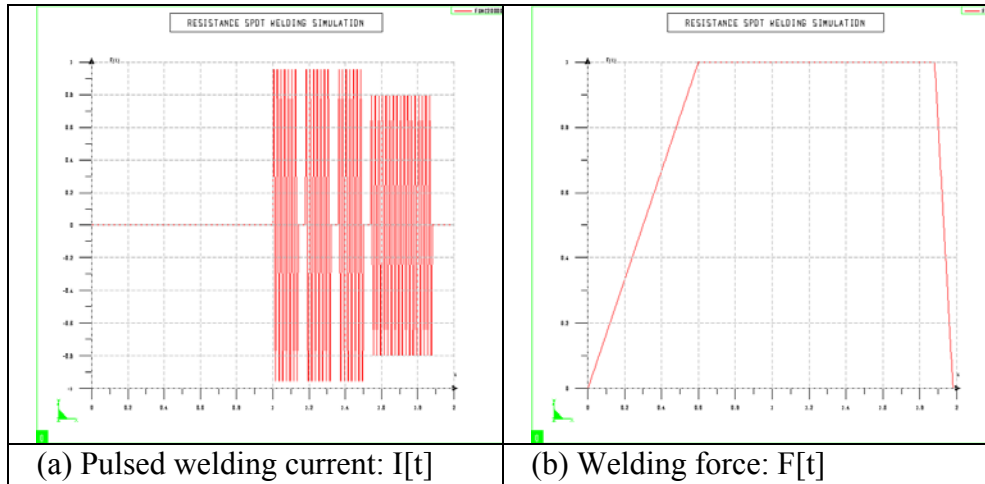


Figure 3: Modeled welding signals used in analysis

Thermal-Mechanical Modeling

The electrode force as illustrated in fig. 3b is modeled from the welding force signal. The mechanical boundary conditions (Ref. 4) are the electrode force applied at the top surface of the upper electrode by assuming a uniform pressure distribution across the annular end and the vertical nodal displacement of annular end of the lower electrode, which is constrained similar manner to that of practical weld. The elasto–plastic Von-Mises criterion without deformation rate dependency is defined for sheet characteristics. The non-linearity due to temperature dependency of sheet properties and contact characteristics including transient computational approach are considered for this study. The three governing equations, namely, the compatibility condition, the constitutive relation, and the equilibrium equation in cylindrical co-ordinate are discussed elsewhere (Ref.5).

EXPERIMENTAL PROCEDURE

Two sheet grades of ARCELOR, a Transformation Induced Plasticity (TRIP) grade and a non-coated drawing quality Low Carbon Steel (LCS) sheet are utilized in this study. Properties of both sheets are given in Refs 6 and 7. The metallurgical examination is conducted only for the low carbon steel sheet joining.

Table 1: Welding schedules utilized in the study

Welding conditions		Current: [kA/Cycles] Force
Elec. dia. (mm)	Configuration	
1) 8	2sheets:(LCS) 2mm-thick	11.2-DC/4(6+2) 400 daN
2) 6	2sheets:(LCS) 2mm-thick	8.97-DC/4(6+2) 400 daN
3) 8	3sheets:(LCS) 2mm-thick	10.6-DC/4(6+2) 450 daN
4) 6	2sheets:(TRIP) 1.46mm-thick	7.80-AC/3(7+2)+6.5×17 500 daN

Welding schedules in table 1 indicate the utilization of pulsed welding current. In the case of TRIP steel sheet joining with electrode face diameter of 6mm., alternating current with a magnitude of 7,80 kA is applied for 3 pulses, each pulse has 7 cycles of welding plus 2 cycles of current shut-off. Furthermore, the post-heating current is then applied for 17 cycles with a magnitude of 6.5 kA. The aim of post-heating current application is to achieve the good quality of residual metallurgical phases and minimize the weld fracture of HSS sheet joining. The as-received sheets are cut to 50×50-mm coupons. Electrode conditioning prior to welding is performed for 50 welding points with bare sheet. The trial welding tests are then conducted in order to determine the expulsion limit. These trial welding conditions are based on the French Industrial Standard (Ref.8), which is considered as welding schedule guideline. The welding schedules, just below the expulsion limit, are used for three welding coupons and for each pulse in order to examine the formation of nugget relating to configurations. The no-expulsion welding of each pulse can be verified from the force and the displacement signal monitoring on the LABVIEW[®] window. The effective current magnitude is obtained from the MIYASHI[®] current signal recorder. Nugget development kinetics can be further examined by sectioning the spot after each interrupted pulse. The polished axial sections of spot welded samples are etched with picric acid to determine the fusion line or the nugget contour. This etchant is suitable for the examination of the fusion zone of low carbon steel spot welds. Quantitative macro-photographic measurements are made for the nugget size.

EXPERIMENTAL RESULTS AND DISCUSSION

Influence of Process Characteristics on Nugget Formation

Nugget development kinetics for two and three LCS sheet joining of 2mm-thick at the end of each pulse is shown in fig. 4. As expected, both the height and the diameter of the nugget increase at the end of the first two pulses. During the third and the fourth pulse, the nugget expands more in diameter than in height. The indentation on the sheet surfaces and the sheet separation can also be observed. The influence of electrode face diameter on nugget formation is demonstrated by comparing case 1 and 2. It is revealed that the increase of electrode diameter face leads to the increase in magnitude of welding current by around 2.2kA if the electrode face diameter of 8 mm is used instead of 6 mm. This is due to the enlargement of contact size reducing the concentration of current flux at faying surface. The utilization of smaller electrode face diameter results in remarkable indentation onto sheet surfaces at the end of welding. Concerning the nugget formation kinetics in the case of two-sheet joining, the occurrence of nugget at faying surface is already observed at the end of the first pulse.

In the case 3, instead of initiating at center of three-sheet assembly, the hot zone originates in superior and inferior regions at the end of the first pulse but the nugget does not start forming yet. For the latter pulses, nugget penetration and development also show a trend similar to that of two-sheet assembly case. The dissymmetry in the upper and the lower nugget diameters can be found before the saturation of nugget diameter at the end of the fourth pulse. However, both symmetrical or dissymmetrical nugget development can be observed for three-sheet joining case. The sheet edge separation between faying surfaces is slightly different. The decrease in current magnitude for the three-sheet assembly comparing to that of two-sheet joining can be explained by the increase of bulk electrical resistance with the increase in number of sheets.

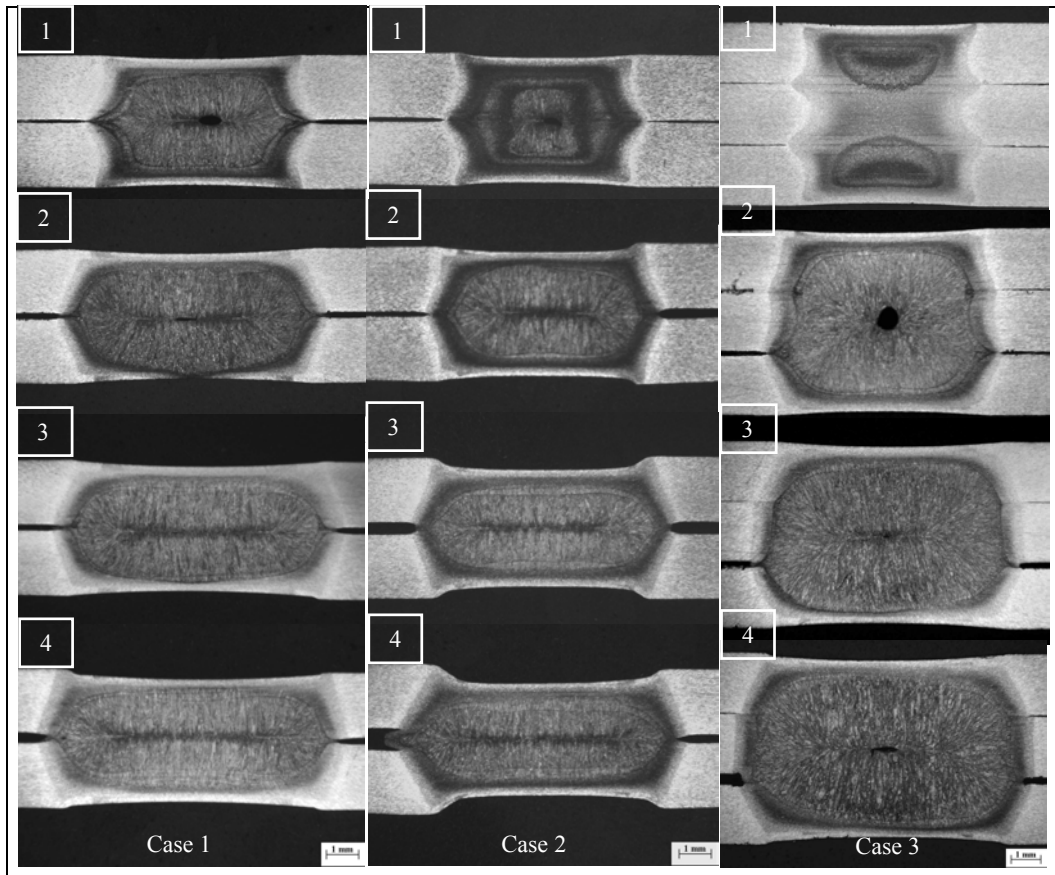


Figure 4: Illustration of nugget formation of two- and three-sheet assembly at the end of each pulse (Number of pulse is indicated on the macro-photograph and see also table 1 for the case study)

COMPUTATIONAL RESULTS AND DISCUSSION

Influence of Process Characteristics on Thermal History

For two-sheet joining case, the temperature history at different positions demonstrates the same dynamic response to the type of welding current used. The drop in temperature during current shut-off can be obviously observed on temperature evolution and markedly seen for the positions located in the nugget region as illustrated in fig.5a. The instantaneous significant increase in heating rate is found during the first pulse, particularly at the beginning. In contrast to the heating rate of weld center for two-sheet joining, there is no significant change in heating rate during the first two pulses for three-sheet joining as shown in fig 5b. An insignificant variation is seen for weld center thermal history during the current shut-off between the first and the second pulses.

For both two- and three-sheet joining cases, There is no variation in thermal history for the positions located far away from the nugget and the HAZ, i.e. $r=8\text{mm.}$, during the weld stage. Unfortunately for the sheet joining with RSW technique, it is not easy to attain the same value of the maximum temperature in order to compare the thermal histories. This is due to the difference in the inherent welding parameters and the configuration used.

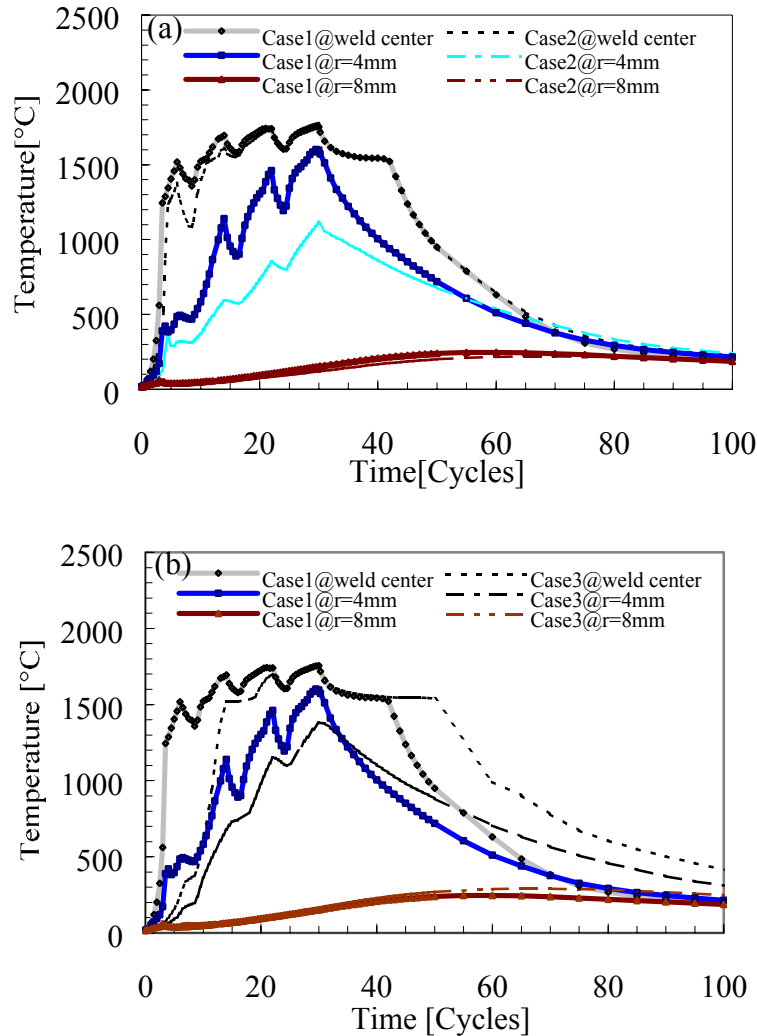


Figure 5: Influence of process characteristics on thermal history considering at the upper limit of weldability lobe

Figure 5a: Influence of electrode face diameter resulting in welding current adaptation and consequently on thermal history

Figure 5b: Thermal history in two- and three-sheet joining cases

Influence of Post-heating Current on Weld Geometries

The nugget geometries and sizes at the end of each pulse in the case of TRIP steel joining are illustrated in fig. 6. It is obvious that the nugget develops until the end of pulsed welding. The peak temperature at the weld center is found at the end of the last or the third pulse. After that, there is no significant evolution of heating rate during the post-heating stage. It is shown that there is no further development in nugget size during the application of post-heating current and this is contrast to metallurgical phase evolution in the HAZ during this supplementary stage. Let us examine a node located inside the nugget and near the fusion line, i.e. node at $y=1,168\text{mm}$ as shown in fig. 7b. The maximum temperature of this node is about 1535°C at the end of the welding process.

The temperature drop can be also observed during the current shut-off. The thermal history of this node increases again during the post-heating stage but with a lower heating rate than that experienced in the assembly during welding. The maximum temperature of this node reaches

about 1354°C at the end of post-heating stage. This reveals that the simulated nugget size at the end of post-heating will be smaller than that obtained at the end of welding. It is worth noting that the appearance of maximum nugget height and diameter is an irreversible phenomenon and only takes place at the end of welding. Therefore, this discussion can be supported by the occurrence of maximum nugget diameter at the end of welding stage with the examination of thermal history. Fig. 6d shows the simulation result of the smaller size of nugget diameter at the end of post-heating stage than that predicted at the end of welding as illustrated in fig. 6c.

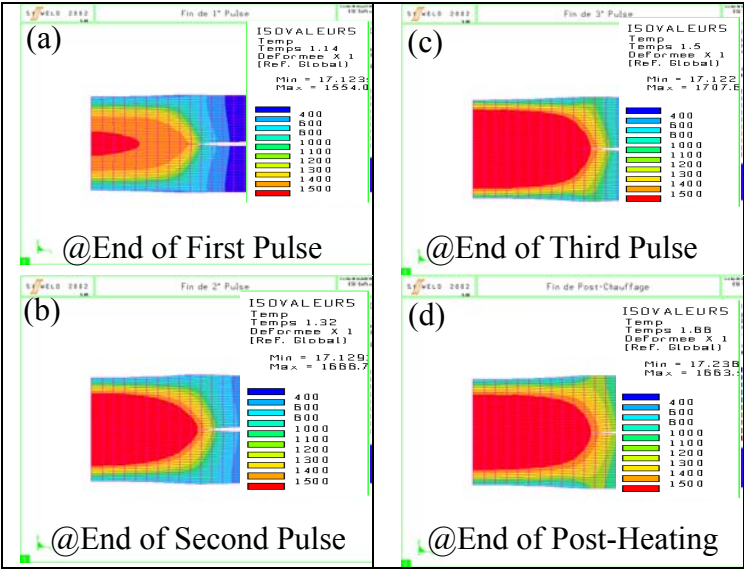


Figure 6: Predicted nugget development kinetics using post-heating current: case4

It is obvious that more important heating rates can be found for the nodes located along the axis than for the nodes located along the radius. However, the temperature history considered at the position located outside and near the HAZ zone, at the position ($r = 4,50\text{mm}$) as shown in fig.7, is increased even during the current shut-off. For the positions located sufficiently far away from the weld center ($r=5.10\text{ mm}$), the drop in their thermal histories cannot be observed and the temperature increases continuously during current shut-off and post-heating stage.

The simulation results reveal that the number of pulses and the magnitude of post-heating current should be prudently selected while practically examining the mechanical and metallurgical properties of weld.

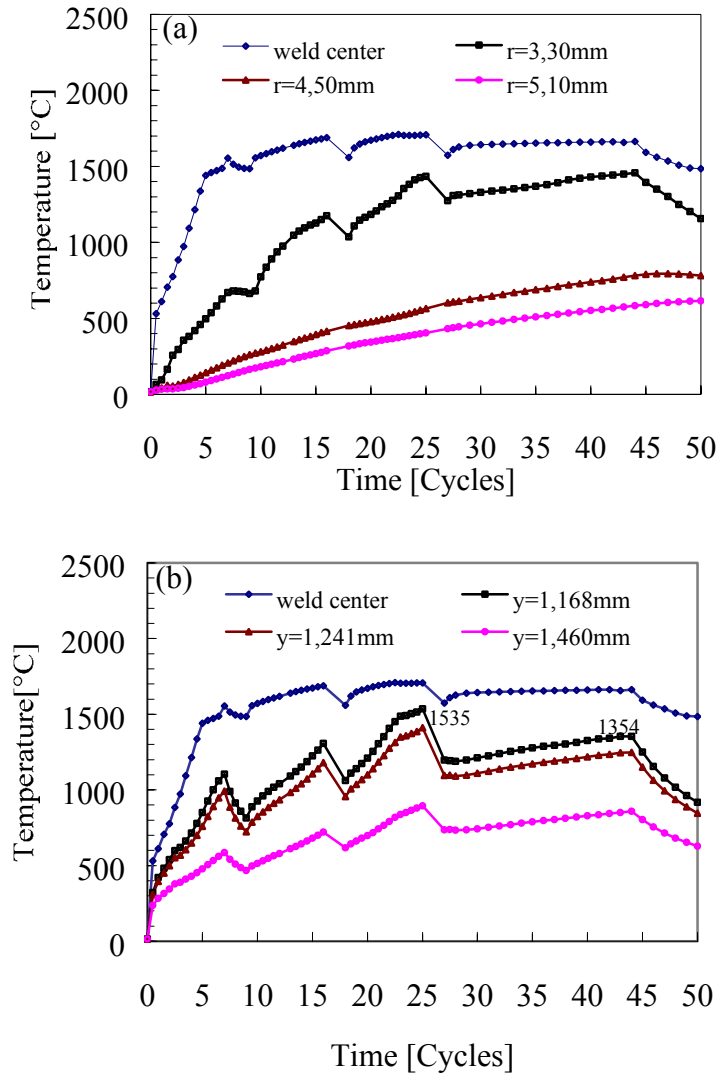


Figure 7: Influence of post-heating current on nugget size at the end of welding: case4

Figure 7a: Average thermal history at different radial position

Figure 7b: Average thermal history at different axial position

Residual Stresses in Assembly

The slide-line mechanical contact element without friction is defined at sheet-to-sheet and electrode-to-sheet interfaces throughout the computation. This contact condition however may not be a very realistic approach for the appearance of nugget at faying surface. In fact, when the nugget starts forming, the faying surface is joined by the molten mold. Therefore, the contact condition associating with the occurrence of nugget should be the sticking contact condition. The novel mechanical contact approach is under development with the modification of mechanical boundary conditions at the different stage of process.

The residual stresses for three-sheet joining case are shown in fig.8.

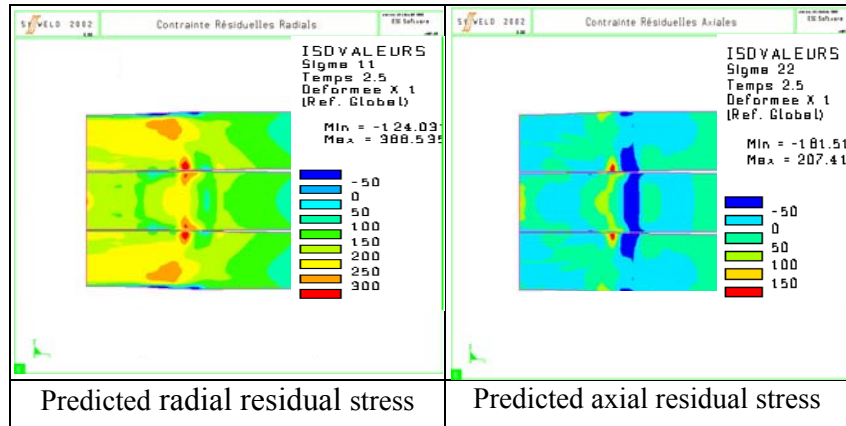


Figure 8: Predicted residual stresses in assembly at the end of process: case 3

EXPERIMENTAL VALIDATION

For three-sheet joining case, the validation is carried out for the quantitative measurement of nugget diameter appearing at the interfaces between the upper-to-middle and the middle-to-lower sheets, namely $D_{upper@exp}$ and $D_{lower@exp}$ respectively.

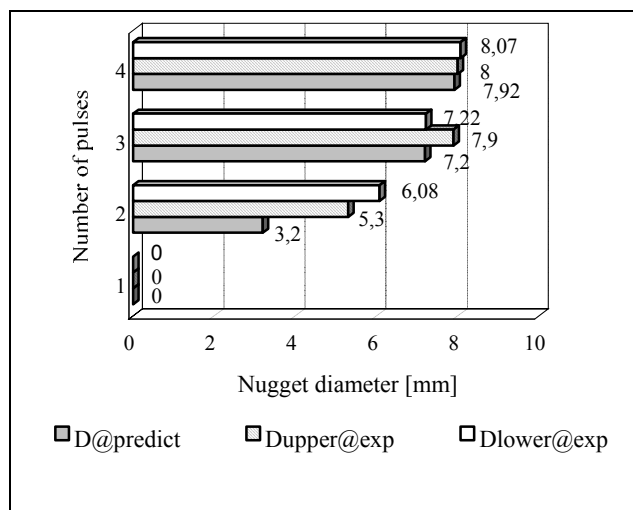


Figure 9: Validation of nugget diameter for three-sheet joining: case 3

Note that the nugget diameters increase significantly during the first two pulses and saturate for the latter stages. Both predicted and measured nugget growth kinetics exhibit similar trend for long welding time. The validation shows a quantitative agreement in nugget diameters at the end of welding, which are of 8mm corresponding to the diameter of electrode face used. However, it is found that there is a discrepancy between the measured and the predicted nugget diameter size, particularly at the end of the second pulse. The measured nugget diameters for the upper-to-middle and the middle-to-lower interfaces are around 5.30 and 6.08mm, respectively. While the simulated nugget diameter sizes are found in an order of 3.2mm and show the effect of planar symmetry as depicted in fig. 9. This discrepancy may be due to the inappropriate electro-thermal contact values at faying surface, particularly for the temperature extending from ambient temperature to 200-400°C. It is understood that the

faying surface contact resistance diminishes rapidly with temperature (Ref. 9) and plays a significant role on the nugget development. These electrical contact resistances also depend strongly on the surface condition of sheet, the welding force and the temperature.

CONCLUSIONS

A finite element analysis based predictive model incorporating an electrical-thermal and thermal-mechanical coupling procedure was applied to study the heavy gauge sheet joining by the RSW technique. This model provides a better understanding of the effects of welding parameters on the nugget development kinetics and on the thermal characteristics in the assembly with the use of pulsed welding current schedules.

The main conclusions of this study are:

- 1) It is experimentally found that the use of the larger electrode diameter leads to an increase in the magnitude of welding current due to a better distribution of current flux and reduces the indentation of electrode face onto the sheets. Concerning three-sheet welding configuration, it well demonstrates the significance of the total bulk electrical resistance of sheet at elevated temperature with the decrease in welding current magnitude. The nugget development exhibits similar trend for long welding time.
- 2) The simulation results show the difference in thermal history experienced in the assembly between two- and three-sheet joining while respecting the upper limit in the weldability lobe before the occurrence of expulsion. The drop in thermal history due to current shut-off can be seen on the temperature evolution for both cases and more markedly in the two-sheet joining case. The thermal history depends strongly on the position in the assembly. For position located sufficiently far away from the nugget and the HAZ regions, there is no impact of current shut-off on the thermal history.
- 3) It is demonstrated that the appropriate selection of the magnitude and the number of post-heating pulses has no effect on the final nugget size obtained at the end of welding. However, the temperature history is slightly increased during the post-heating stage for every position in the assembly.
- 4) The validation result shows a good agreement for the final nugget size at the end of welding in the case of three-sheet joining. But the discrepancy in nugget diameter size development can be observed during the first two pulses before the saturation of nugget. This may be due to the inappropriate values of electrical contact resistances introduced at faying surface. Electrical contact resistance determination will be further conducted in order to evaluate the contact characteristics.

ACKNOWLEDGEMENTS

The authors would like to express their grateful acknowledgement to Messieurs G. RIGAUT, and J. CLAEYS, the director of the Metallurgical Development and Research Center and the head of resistance welding section, respectively, for their input during the paper preparation. Thanks also to J.P. DOUILLY, who performed all spot weld experiments in this study. The authors wish to thank C. DJENKAL and D. MALEWICZ for their educative advice during metallurgical preparation and investigation. The partial financial support of Association Nationale pour la Recherche et la Technologie (CIFRE educational program) is gratefully acknowledged.

REFERENCES

1. Peterson, W. May 15-17 2002. Methods to minimize the occurrence of interfacial fractures in HSS spot welds. Sheet metal welding conference X. Sterling Heights, MI.
2. Khan, J.A.; Xu, L.; and Chao, Y.J. 1999. Prediction of nugget development during resistance spot welding using coupled thermal-electrical-mechanical model. Science and technology of welding and joining. Vol. 4, No.4: 201 to 207.
3. Sun, X.; and Dong, P. Aug. 2000. Analysis of aluminum resistance spot welding processes using coupled finite element procedures. Welding research supplement: 215-s to 221-s.
4. Srikunwong, C.; Dupuy, T.; and Bienvenu, Y. Nov., 2001. A decoupled electrical-thermal and mechanical model for resistance spot welding. 15th annual conference of mechanical engineering network of Thailand. Bangkok, Thailand. Vol.2: 76 to 84.
5. Murakawa, H.; Kimura, F.; and Ueda, Y. 1997. Weldability analysis of spot welding on aluminium using FEM. Mathematical modeling of weld phenomena 3: 944 to 966.
6. Thiéblemont, E. 1992. Modélisation du soudage par points. Ph.D. dissertation. L'Institut National Polytechnique de Lorraine. (in French)
7. Bobadilla, M.; Niederleander, M.; Nuss, C.; Perrin, G.; and Selaries, J. Juin 1994. Données thermiques pour différentes familles d'acier. Rapport interne IRSID, Groupe Usinor. (in French)
8. Caractérisation de la soudabilité par résistance par point de produits plats revêtus ou non, Déc. 1994, Normalisation française A87-001. (in French)
9. Vogler, M.; and Sheppard, S. June 1993. Electrical contact resistance under high loads and elevated temperatures. Welding research supplement: 231-s to 238-s.